New Phytologist

Pit membrane structure is highly variable and accounts for a major resistance to water flow through tracheid pits in stems and roots of two boreal conifer species

Paul J. Schulte[1], Uwe G. Hacke[2] and Amanda L. Schoonmaker[3]

[1]School of Life Sciences, University of Nevada – Las Vegas, Las Vegas, NV 89154, USA; [2]Department of Renewable Resources, University of Alberta, Edmonton, AB, Canada; [3]Boreal Research Institute, Northern Alberta Institute of Technology, Peace River, AB, Canada

Author for correspondence:
Paul J. Schulte
Tel: +1 702 895 3300
Email: paul.schulte@unlv.edu

Received: *18 January 2015*
Accepted: *29 March 2015*

New Phytologist (2015) **208:** 102–113
doi: 10.1111/nph.13437

Key words: computational fluid dynamics, hydraulic resistance, pit membrane, torus–margo pits, xylem.

Summary

- The flow of xylem sap in conifers is strongly dependent on the presence of a low resistance path through bordered pits, particularly through the pores present in the margo of the pit membrane.
- A computational fluid dynamics approach was taken, solving the Navier–Stokes equation for models based on the geometry of pits observed in tracheids from stems and roots of *Picea mariana* (black spruce) and *Picea glauca* (white spruce).
- Model solutions demonstrate a close, inverse relationship between the total resistance of bordered pits and the total area of margo pores. Flow through the margo was dominated by a small number of the widest pores. Particularly for pits where the margo component of flow resistance was low relative to that of the torus, pore location near the inner edge of the margo allowed for greater flow than that occurring through similar-sized pores near the outer edge of the margo.
- Results indicate a surprisingly large variation in pit structure and flow characteristics. Nonetheless, pits in roots have lower resistance to flow than those in stems because the pits were wider and consisted of a margo with a larger area in pores.

Introduction

Conifer trees are among the largest living organisms (Koch *et al.*, 2004) and their xylem transport pathway from roots to the leaves relies on water flow through tracheids. Limitations imposed by the hydraulic pathway are thought to be the major constraint on the maximum heights attainable by conifers (Koch *et al.*, 2004), although other factors may contribute (Ryan & Yoder, 1997; Woodruff *et al.*, 2004; Jensen & Zwieniecki, 2013). Tracheids are short conduits (a few mm in length) relative to vessels, as found in most angiosperms, and flow from cell to cell depends on the presence of pits in the tracheid walls. The structure of pits in many conifers is of great significance because of the presence of a torus that appears to be able to seal the pit when one tracheid contains air, thus preventing the spread of an embolism (Zimmermann, 1983; Sperry & Tyree, 1990; Hacke *et al.*, 2004). Mathematical models of the torus displacement in response to pressure by Chapman *et al.* (1977) support the idea that the torus could act as a valve, although they suggest that sufficiently large flows would also close the valve. In addition, the region of the pit membrane surrounding the torus contains particularly large pores as compared with the pit membranes typical in angiosperms (Bauch *et al.*, 1972; Sperry & Hacke, 2004; Pittermann *et al.*, 2005; Dute *et al.*, 2008). Therefore this combination of a margo with large pores and the pit-sealing capability of the torus allows for conifers to have a very efficient transport pathway despite the lack of wide, low-resistance vessels (Hacke *et al.*, 2004; Pittermann *et al.*, 2005; Domec *et al.*, 2008).

As suggested from a number of experimental and theoretical perspectives, the distribution of margo pores (numbers and sizes) should play a prominent role in determining the low resistivity nature of the pit margo upon which the efficient hydraulic nature of conifer xylem depends. The pits in conifers appear to constitute > 50% of the total pathway resistance for the xylem (Domec *et al.*, 2006; Pittermann *et al.*, 2006; Sperry *et al.*, 2006; Schoonmaker *et al.*, 2010), and therefore understanding the role played by the distribution of margo pores should be of fundamental importance. Several studies have attempted to model the pit membrane (Lancashire & Ennos, 2002; Hacke *et al.*, 2004; Domec *et al.*, 2006); however, the margo structure is complicated and difficult to approximate with a physical system.

In addition to pit structure being significant for flow, work with boreal forest conifer species has demonstrated that pit membrane structure (see Fig. 1 for terminology) is important in the ability of tracheids to isolate embolisms (Hacke & Jansen, 2009). Their study found that the diameter of the pit aperture scaled closely with torus diameter, possibly related to the ability of the torus to provide a seal against the pit borders. Increasing

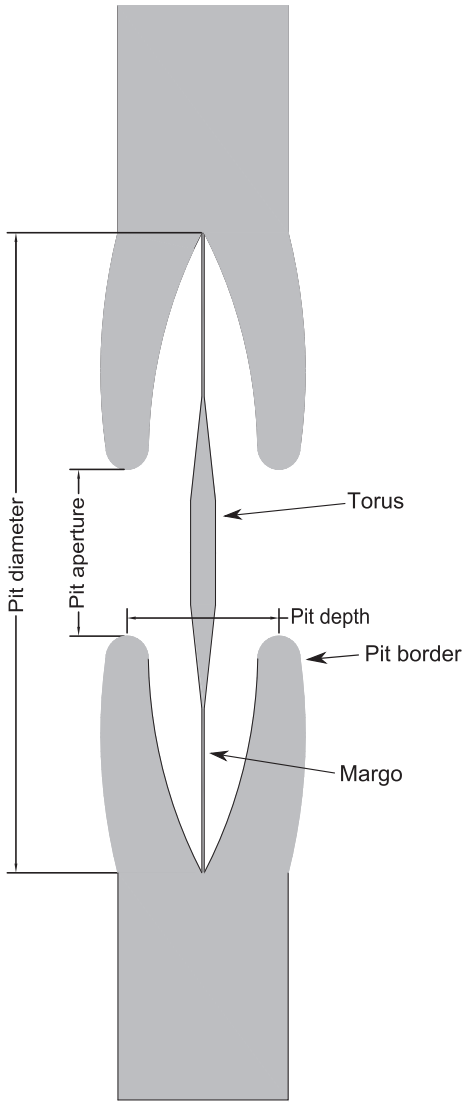

Fig. 1 Conceptual model of a *Picea glauca* or *Picea mariana* tracheid bordered pit pair viewed in cross-section, showing the terminology used to refer to various pit components and dimensions. The torus and margo structures are often collectively referred to by the term 'pit membrane'.

vulnerability to embolism was associated with a lower ratio of torus diameter to pit aperture diameter and also with the pit depth (distance from pit borders on one side, through the torus, to the pit borders on the other side). In addition, pits were substantially wider in roots than in stems. Many of these trends have also been observed in other studies (Pittermann *et al.*, 2006, 2010; Domec *et al.*, 2008; Bouche *et al.*, 2014). Therefore, the dimensions of various components of conifer pits are associated with both resistance to flow and vulnerability to embolism.

A recent approach to modeling flow through pits has been based on computational fluid dynamics (Schulte, 2012a), commonly used by engineers in assessing flow through structures, including 'lab on a chip' devices and other microfluidics processes. Although demonstrating the development of this approach, the sample size used by Schulte (2012a) was small: one pit model was developed each from a *Picea mariana* grown in sun-exposed and shaded understory locations. For the two models developed, estimates could be made of the role of structural details such as the margo pore sizes and their distribution within the margo. The objectives of the present work were to utilize the modeling approach to explore the variation in structure of individual pits and relate this variation to flow resistance through the pits, and to compare two boreal forest conifers (*P. mariana* and *Picea glauca*) and consider pits in tracheids of stems as well as roots for these two species. Among the conifers with characteristic bordered pits, including a torus in the pit membrane, *P. mariana* (black spruce) and *P. glauca* (white spruce) are widespread across the boreal forests of Canada. White spruce may be considered both an early- and a late-successional shade-tolerant conifer with broad ecological amplitude, although it is most commonly found in medium to rich sites with moderate moisture regimes (Klinka *et al.*, 2000). In Alberta, at low elevations, it often grows in mixtures with aspen (*Populus tremuloides*), and at higher elevations it is often the dominant tree species along with lodgepole pine (*Pinus contorta*). Black spruce is considered to be even more shade-tolerant than white spruce (Klinka *et al.*, 2000) and also has broad ecological amplitude, although it is most commonly found on very poor to poor sites that tend to be moist to wet. Given previous work with these and other conifers (Domec *et al.*, 2006; Pittermann *et al.*, 2006; Hacke & Jansen, 2009), we hypothesized that pits from roots would present lower flow resistance because the margo would be the dominant source of flow resistance and this resistance attributable to the margo would be lower, owing to the presence of a greater number of, and wider, pores within the margo. Tracheids in roots are typically wider and longer than those in branches (Sperry & Ikeda, 1997; Hacke *et al.*, 2004; Dunham *et al.*, 2007) and so a lower pit resistance in roots might keep the relative contribution of the tracheid lumen and pits to overall xylem resistance roughly comparable among both roots and stems, a characteristic that has been suggested for tracheids in general (Pittermann *et al.*, 2006; Choat *et al.*, 2008).

Materials and Methods

Plant materials

For the present study, trees of *Picea glauca* (Moench) Voss and *Picea mariana* (Mill.) BSP. were collected in four locations: at the University of Alberta Farm, south of Edmonton, Alberta (53°24′44.8″N, 113°32′32.0″W), at two locations 50 km east of Peace River, Alberta (56°23′39.0″N, 116°53′35.6″W and 56°23′2.2″N, 116°46′20.5″W), and at a location 55 km south of Valleyview, Alberta (54°32′22.1″N, 117°00′50.0″W). Site elevation ranged from 615 to 802 m. Trees were open-grown and fully exposed to light (dominant or codominant). The collection of samples from multiple sites was necessary, as these species typically occupy different forest types. Samples were collected from trees that varied in height from 1.5 to 5 m, to ensure that stem samples could be taken from the upper third of the tree crown. Stem samples were from 1- to 2-yr-old branches and were collected with hand clippers or pole cutters (for taller individuals). Roots were sampled by digging from the base of the tree and

following the root outward until it reached the target diameter (0.5–1.0 cm). Typically the root was sampled within 1–2 m of the tree base and was occasionally a first-order root but more often a second-order root. Root and stem samples were collected from different trees and are thus independent. Six to eight samples were collected from individuals of each species and organ and placed in plastic bags and stored at 4°C within 6 h of collection. Whenever possible, samples were processed within 3–4 d of collection or stored frozen until required for scanning electron microscopy (SEM).

The terminology for various features of the bordered pits studied in this paper is given in Fig. 1.

Electron microscope imaging

For SEM imaging of pit membranes, one must always consider sample preparation techniques with respect to the possible generation of artifacts. Jansen *et al.* (2008) considered several sample preparation methods for observing *Pinus wallichiana* pit membranes. Methods such as liquid nitrogen/freeze drying, hydrogen peroxide or acetone treatment resulted in differences in observed pit membrane pore sizes. Methods involving ethanol resulted in more porous membranes than air drying, but others have found the opposite effect (Schoonmaker *et al.*, 2010; Plavcová *et al.*, 2011). Plavcová *et al.* (2011) found that air drying alone damaged pit membranes; however, taking samples through a gradual ethanol series up to 100% followed by air drying resulted in reduced damage and images with smaller pit membrane pores. Schoonmaker *et al.* (2010) used a similar approach, as it minimized pit aspiration compared with air drying alone. For the present study, wood samples were cut into *c.* 1-cm-long segments and initially split in half. Samples were soaked in distilled water for 1–5 d (a shorter time for fresh material and a longer time for frozen material). Following soaking, samples were put through a dehydration series (30, 50, 70 and 90% ethanol for 0.5 h at each concentration) in order to remove water. Finally, samples were placed in 100% ethanol overnight and air-dried for a minimum of 24 h. Samples were carefully split radially again to expose new pits. Care was taken to allow the wood grain to split naturally by only initially inserting a blade *c.* 0.1 cm into the wood section and using pressure to split the pieces apart. This was more effective at exposing pits than intentionally cutting all the way through with a blade. Split samples were mounted on aluminum stubs with silver paint, and a thin layer of chromium was applied with a sputter coater for 1 min. Pit images were collected with a JEOL 6301F field-emission scanning electron microscope (Jeol, Tokyo, Japan) at an accelerating voltage of 2.5 kV. Transmission electron microscopy (TEM) sample preparation and imaging for measuring pit chamber overall shapes was carried out as described by Hacke & Jansen (2009). Briefly, TEM samples were cut into 2 mm^3 blocks and fixed overnight in Karnovsky's fixative. Specimens were then buffer-washed, dehydrated, and embedded in LR White resin (London Resin Co., Reading, UK). Ultrathin sections between 60 and 90 nm were cut using a diamond knife. Observations were carried out using a JEM-1210 TEM (Jeol) at 80 kV accelerating voltage.

Modeling approaches

Fundamentals The general approach for describing fluid flow relies on the Navier–Stokes equation, which is based on Newton's second law through a combination of terms describing the acceleration of the fluid and forces acting on the fluid (Munson *et al.*, 1990). These forces include pressure and shear forces within the fluid. An expression of this equation for steady-state flow (constant velocity with respect to time) is:

$$\rho(\mathbf{V} \cdot \nabla\mathbf{V}) = -\nabla p + \mu\nabla^2\mathbf{V} \qquad \text{Eqn 1}$$

where $\mathbf{V}$ is the velocity vector (m s^{-1}), p is the pressure (Pa), μ is the fluid dynamic viscosity (Pa s) and ρ is the fluid density (kg m^{-3}). A continuity expression is supplied assuming an incompressible fluid with constant density:

$$\nabla\mathbf{V} = 0 \quad \text{or} \quad \frac{\partial u}{\partial x} + \frac{\partial v}{\partial y} + \frac{\partial w}{\partial z} = 0 \quad \text{(3D case)} \qquad \text{Eqn 2}$$

In both equations, the symbol ∇ refers to a partial gradient with respect to the spatial variables (x, y, z for a three-dimensional (3D) model). Further details regarding boundary conditions and the applicability of this approach for structures at the spatial scales found in pits are described in Schulte (2012a).

Fluid flow models were developed using the Comsol Multiphysics software (Comsol Inc. Los Angeles, CA, USA), a general program for the solution of partial differential equations (here solving the Navier–Stokes and continuity equations), including development of the model geometry and its finite element mesh. Detailed regions of the model such as the pit border and margo pores were drawn in AutoCAD (Autodesk Inc. San Rafael, CA, USA) and imported into the model within the Comsol software. Simulations utilized a Dell T7500 64-bit workstation with two quad-core processors and 128 GB of memory. Solution requirements varied from 2 to 4 h and 60–120 GB of memory.

Integration of images into model software Model development was based on TEM and SEM images. The model portion for the overall pit chamber shape was based on TEM images (seven to 10 images per species and organ). SEM images showing detail of the pit membrane (four to five images per species and organ) were used to develop the margo portion of the pit models. Thus, complete 3D models of pits (four to five independent models per species and organ based on their geometry) were developed with a pit chamber shape based on TEM images and a margo with pores from the SEM images. From viewing large numbers of TEM images of the pit chamber shapes, it was clear that considerable variation was present with respect to the shapes of pit borders and associated dimensions. Whereas the model portion for the margo was based on SEM images of the margo in a face-on view, a TEM view showing pit border shapes and dimensions in cross-section for the same pit was not obtainable. Therefore a consensus model of the pit chamber for each species and plant organ was based on the seven to 10 TEM images per species and organ (see Supporting Information Fig. S1). Each TEM image

was imported into an AutoCAD drawing and scaled based on the reference scale line in the image. The outline of pit borders was traced with AutoCAD 'polylines' (combinations of straight-line segments and arcs) and dimension lines were drawn to measure pit features such as diameter and aperture. Consensus models (representing a pit of average dimensions; Fig. 2) were then used for creating the 3D pit chamber in the fluid flow model (imported into the Comsol Multiphysics program). The combination of TEM and SEM imaging represents a constraint on our ability to produce a model of a specific pit because a TEM view of the pit chamber shape was not obtainable for the same pit that was imaged by SEM for the margo structure; hence the need for such consensus models. On the other hand, previous work (Schulte, 2012a) suggests that the pit aperture (as formed by the pit borders) component of total pit resistance is relatively minor compared with the margo resistance, and thus the variation apparent in pit chamber shapes will be reduced in significance when the margo is included in the 3D models.

The SEM image showing a face-on view of the margo and torus was imported into an AutoCAD drawing and scaled based on the reference line in the image. Next, the AutoCAD polyline tool was used to draw (by tracing over the image) polygons corresponding to each pore (the number of pores varied from 500 to 2500 depending on the individual image). We attempted to use images with an intact, undamaged margo, but in many cases portions of the margo were damaged: 13 of the 19 images showed damage to areas ranging from 6 to 35% of the margo (the mean damaged area for these 13 images was 20.6%). Damage was readily apparent from the presence of small stubs of margo fibrils extending out into an often unusually large open pore. This damage, presumably an artifact of sample preparation, occurred over one or two areas and was not scattered throughout the margo. For cases with partial damage to the margo, pores were copied from intact regions radially opposite the damaged region. The AutoCAD drawing of the margo pores was then imported into the 3D pit chamber model in the Comsol Multphysics software. The thickness of the margo (depth of margo pores) was 50 nm (as used in Schulte, 2012a). The solution of this equation system provided flow velocities (x, y and z components) and fluid pressure as based on the established boundary conditions: a pressure of zero at the model outlet and a fixed inlet velocity of 0.1 mm s^{-1}. The flow regime was dominated by viscous forces (Reynolds number $\ll 1$), and so, for example, doubling the inlet velocity led to a doubling of pressure drops within the model. Calculations of hydraulic resistance (pressure divided by flow) would thus give values independent of the model inlet velocity – an expectation that was confirmed by repeated runs of models with different inlet conditions.

Statistical analyses

The effects of species (*P. mariana* vs *P. glauca*) and plant organ (root vs stem) on various anatomical and fluid flow characteristics were analyzed by two-way ANOVA using the SPSS program (version 20). For cases where the assumption of homogeneity of variances was not satisfied, the Scherer–Ray–Hare nonparametric test was implemented within SPSS as described by Dytham (2011). A limitation in the number of replicate samples for both species and organs among the various sample sites did not allow us to address site as a random effect.

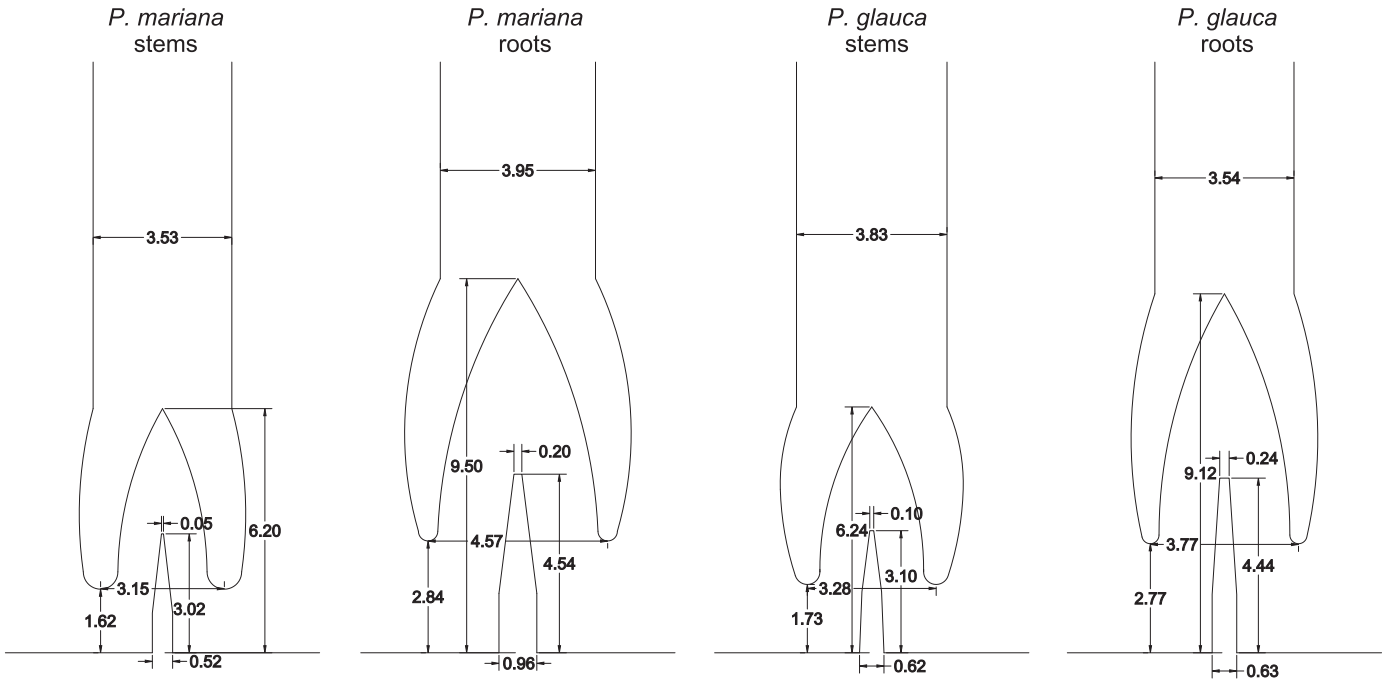

Fig. 2 Consensus models for the two species (*Picea glauca* and *Picea mariana*) and two organs studied (showing one-half of the pit). All dimensions are in μm. These models were used as the basis for the pit chamber in each three-dimensional model. Slight adjustments were made to the pit diameter to match the width of the pit membrane in the scanning electron microscope (SEM) image used to create the margo pores.

Results

For the purpose of estimating the roles of various pit components, such as the pit borders, torus, and margo, as sources of resistance to fluid flow through the pits, models were constructed without pit borders, and then with the borders, the torus, and finally the margo added to the model. In general, the narrow pit aperture formed by the pit borders created a region of high flow velocity (Fig. 3). The figure shows only one model solution (here, from a *P. glauca* stem pit), but other models reflected similar flow profiles within the pit chamber. It is also clear from this figure that fluid flow between the pit borders and the pit membrane occurs with higher velocity in portions of the membrane near the torus as compared with flow through the narrow spaces at the outer edge of the membrane.

Anatomical differences between species and organ

Considerable anatomical variation was present between the two species and between the root and stem organs (Table 1). Pits were significantly wider in roots than in stems (1.6-fold), but significant differences were not found between the two species. The pit aperture was also significantly wider in roots than in stems (1.7-fold), but again species differences were not significant. The total area of pit membrane pores (but not the number of pores per pit membrane) was significantly greater in roots than in stems (1.9-fold). *Picea mariana* pit membranes had a significantly lower total pore area (1.6-fold), but the number of pores in the margo was not significantly different in comparison to *P. glauca*.

Flow velocity through bordered pits

The solution of each pit model provided fluid velocity and pressure at all points within the model. Plots were obtained for each model of flow velocity through the margo pores on a plane parallel to the pit membrane (Fig. 4). Also apparent in Fig. 4 is the wide variation in margo structure, even within each species or organ. As noted previously, these results are not intended to suggest absolute flow velocities within margo pores under any particular flow state occurring in an intact plant in the field. However, comparisons of velocity within a particular margo or between different pits are valid. Maximum flow velocity within a pit was greater in the stem pits than in the root pits, because stem pits were narrower than root pits. Within an individual pit, flow was strongly focused on the larger pores in the margo. For each model, the cumulative flow through the largest 25 margo pores was calculated. This quantity averaged 40% of total flow through the margo for all models, although there were significant differences between roots and stems (36 and 45%, respectively) and significant differences between *P. mariana* and *P. glauca* (33 and 48%, respectively). In addition, it can be seen that higher flow was focused on the inner region of the margo. Quantitative comparisons of pore area and flow through that pore (see Figs S2, S3) suggest that for pits with a strong resistance component associated with the torus, pores of equivalent area can have as much as a twofold greater flow if located on the inner edge of the margo as opposed to the outer edge. If the margo component of resistance was dominant, then such effects of pore location were less apparent.

Resistance to flow through bordered pits

The total resistance to flow presented by each pit was calculated from the model pressure drop ($p_{inlet} - p_{outlet}$) divided by the volume flow through the model (varied slightly depending on the model from 7.04 to 7.06E–14 $m^3 s^{-1}$). Pit resistance was strongly affected by pit diameter and also the total area of all the pores in the pit membrane (Fig. 5). Wide pits had lower total flow resistance; a clean split between root and stem pits with respect to diameter (Fig. 5a) corresponded to a nearly complete

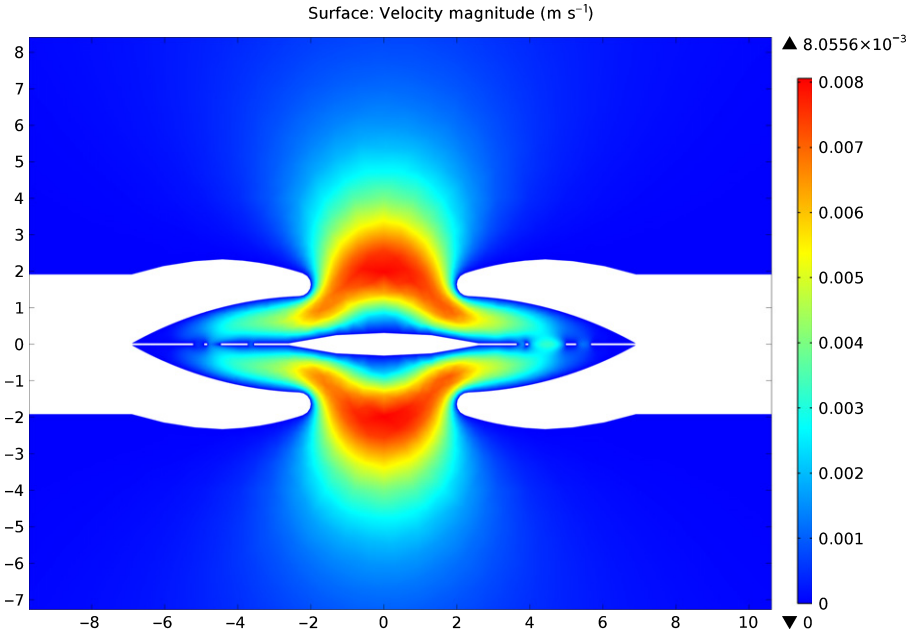

Fig. 3 Representative model solution showing flow velocity through the pit chamber for a model with pit borders, torus, and margo present. The particular solution is shown for a *Picea glauca* stem model, but other models had a similar general appearance in this type of plot. Numbers along the bottom and left edge indicate distances in μm from the center of the pit.

Table 1 Anatomical data for the pits as modeled

	Picea mariana		*Picea glauca*		Significance at $P = 0.05$	
Variable	Stem	Root	Stem	Root	Species	Organ
Pit diameter (μm)	11.400 (0.636)	18.200 (1.043)	11.450 (0.885)	18.440 (1.147)	No	Yes
Pit aperture (μm)	3.336 (0.177)	5.384 (0.301)	3.275 (0.287)	5.744 (0.227)	No	Yes
No. of pores	1081.6 (101.0)	1790.2 (258.5)	863.75 (59.6)	1155.2 (263.3)	No	No
Total pore area (μm^2)	26.932 (4.764)	44.415 (6.119)	33.763 (7.909)	76.339 (9.081)	Yes	Yes

Data are the means of selected anatomical characteristics for pits of *P. glauca* and *P. mariana* built into the complete three-dimensional pit models based on scanning electron microscopy images of the pits, with $n = 4$–5 for each combination of species and plant organ. The SE of the mean is shown in parentheses. Significance tests are from two-way ANOVA, except for the 'no. of pores' measure, where the homogeneity of variances test indicated that the nonparametric Scherer–Ray–Hare test was needed.

clustering of stem pits as having higher flow resistance. In addition, the clear linear relationship between pit resistance and pit diameter observed in stems was absent in roots (Fig. 5a; for stems, this relationship had an $r^2 = 0.538$; for roots, the relationship had a nonsignificant $r^2 = 0.081$). Pits with a greater total pore area in the margo had lower flow resistance (Fig. 5b). Indeed, the apparent inverse relationship (shown in the inset in the upper right of Fig. 5b) is supported by an $r^2 = 0.862$ for a corresponding linear relationship between the inverse of total resistance (hydraulic conductance) and total pore area.

The total resistance of the bordered pits to flow was significantly greater for pits from stems (*P. mariana*, 98.70E+14 Pa s m^{-3}; *P. glauca*, 81.06E+14 Pa s m^{-3}) than from roots (*P. mariana*, 42.06E+14 Pa s m^{-3}; *P. glauca*, 19.95E+14 Pa s m^{-3}). The species difference in these cited values for pit resistance was not significantly different (nonparametric Scherer–Ray–Hare test, $P = 0.241$). The margo resistance per unit area (r_{margo}) was calculated from the margo resistance multiplied by the margo area (see Table 2 for formulae). This parameter was significantly lower in *P. glauca* (stems, 0.268 MPa s m^{-1}; roots, 0.222 MPa s m^{-1}) than in *P. mariana* (stems, 0.434 MPa s m^{-1}; roots, 0.686 MPa s m^{-1}). Differences in margo resistance per unit area between root and stem organs were not significant.

Components of overall pit resistance: pit aperture, torus, and margo

For each pit that was modeled in this study, models were developed for a pit without borders, with borders forming an aperture, with a torus present in addition to the aperture, and with a margo (containing the margo pores) connecting the torus to the pit edge. Calculation of the various resistance components utilized formulas shown in Table 2. This procedure allowed us to calculate the role of each pit component in determining the total pit resistance (Fig. 6). For both the two species and the two organs, the pit aperture was a relatively small component: 5–22% of the total. The margo (pit membrane pores) fraction of total pit resistance was dominant (averaging 56, 76, 44 and 47% of the total for *P. mariana* stems, *P. mariana* roots, *P. glauca* stems, and *P. glauca* roots, respectively). As such, the margo fraction of pit resistance was significantly greater for the pits in roots than in stems and also for the pits in *P. mariana* compared with those in *P. glauca*. With all three components combined, the boxplot for total pit resistance (Total, Fig. 6) shows the large variation among pits, particularly for stems of *P. mariana* and *P. glauca*, but also for *P. mariana* roots. The higher total resistance of stem pits as compared with root pits was also apparent (Total, Fig. 6) and this difference was significant, as noted in the previous paragraph.

Discussion

Solutions of the models for pits from *P. mariana* and *P. glauca* roots and stems demonstrate a number of general similarities with respect to flow through the various structures within the bordered pits. As noted by Schulte (2012a), the presence of a torus diverts flow into the regions between the pit borders and ultimately through the pores in the margo. The flow velocity was greatest where flow was confined either in the pit aperture regions or within individual pores of the margo. Similar flow profiles within the pit chamber were noted by Valli *et al.* (2002) in their computational models that treated the margo as a set of randomly oriented fibers or as a homogeneous medium. In the present study, the area of an individual pore in the margo had a strong effect on the flow velocity and total volume flow within that pore. Although as many as 2500 pores were included in each pit model, on average for all pit models, the largest 25 pores accounted for *c.* 40% of total flow. Pittermann *et al.* (2010) also suggested that a small number of large pores in the margo might have a great impact on overall flow and membrane resistance to flow. Pore location radially (near the torus or near the outer edge of the margo) also affected the flow through that pore. Larger pores tended to be located closer to the torus and, furthermore, such locations also led to high flow because of the greater distance between the margo and the pit borders at that location. In the opposite sense, flow through pores near the outer edge of the margo encountered greater resistance upstream and downstream from that pore because of the narrow space between the pit borders near the edge of the pit membrane. Therefore the presence of wider pit membrane pores near the inner side of the margo may be of adaptive significance because those pores would contribute to flow to a greater extent than similar pores located near the outer edge of the margo. The presence of a large number of small pores at the outer edge of the margo, hence a region of greater margo material, may be of greater significance for mechanical support of the torus.

New Phytologist

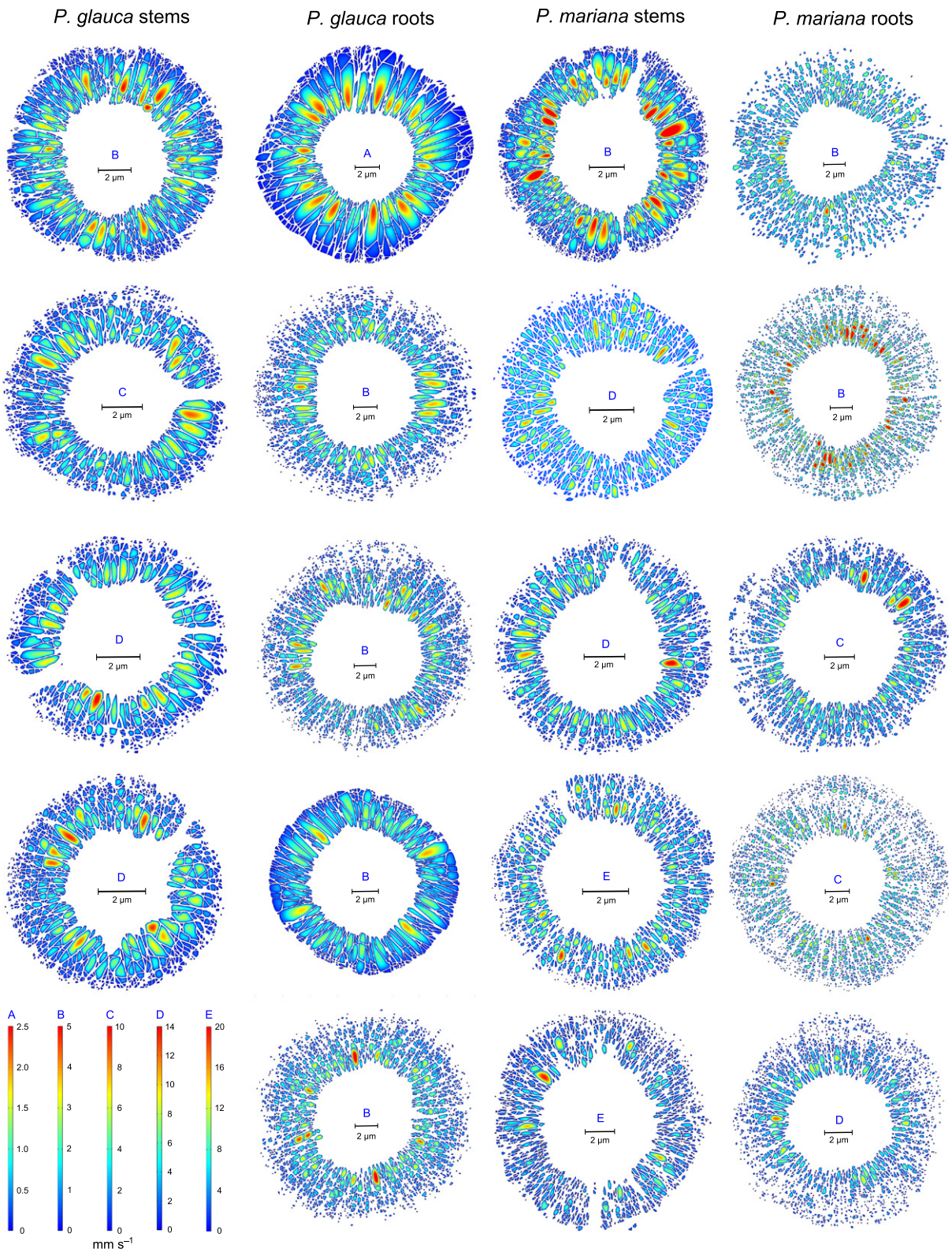

Fig. 4 Flow velocities within the pit membrane pores on a plane parallel to the pit membrane and midway along the pore depth for pits of *Picea glauca* and *Picea mariana*. Shown are the four to five complete pit models developed per species and plant organ to highlight variability in pit membrane structure. The spatial scale and range of flow velocities varied among the pits, and so different color scales were chosen to make flow variation within an individual pit visible (with the same color scale for all pits, many of them showed no variation in color across the pit). The spatial scale and a letter indicating the color range are shown in the middle of each pit, with corresponding color scale ranges (mm s^{-1}) shown at the bottom left of the figure.

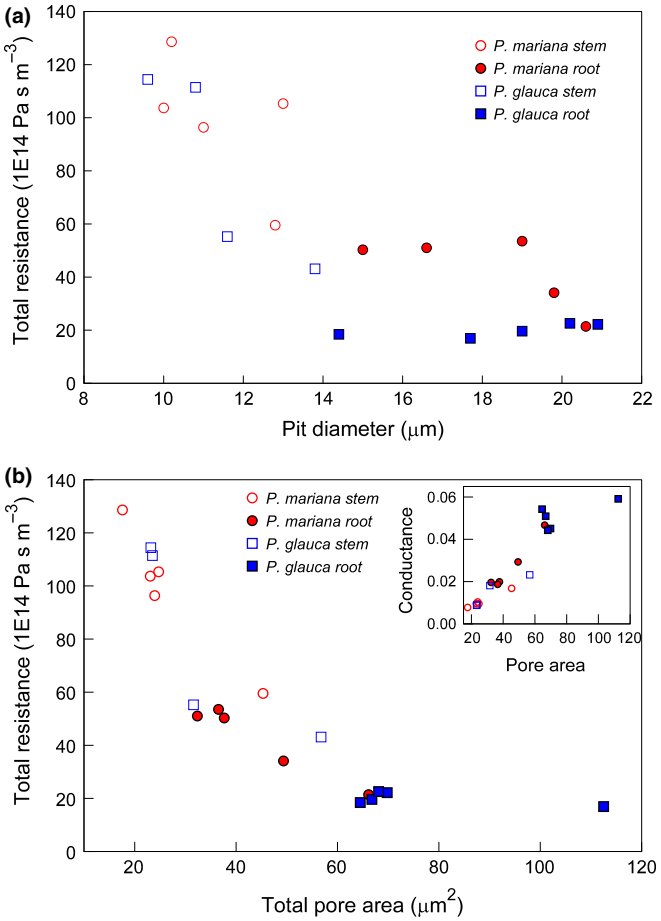

Fig. 5 Total resistance through the pit models for *Picea glauca* and *Picea mariana* as composed of pit borders, torus, and margo as a function of: (a) pit diameter, and (b) the combined area of all margo pores. The inset in (b) shows a related relationship between flow conductance (inverse of resistance) and total pore area.

Pit depth appears to be an important characteristic because it will affect the spacing between the pit border and the margo, which will in turn affect the distribution of flow across the margo. If the spacing is small, a pore's location near the outer edge of the margo would be disadvantageous for flow. This characteristic arises because for low Reynolds (viscosity-dominated) flow, proximity to a no-slip wall leads to high shear forces in the fluid. Using the same reasoning, the degree of curvature of the pit borders would be significant for increasing the space between the pit border and the margo. Schulte (2012a) concluded that this was a general characteristic of bordered pits, but with the greater sample sizes in the present study, it became clear that the importance of pore location depends on the degree of dominance of the margo component; for pores of a given size, their radial location becomes less significant as the margo component becomes more dominant. Hypothetically, a curved border (curved away from the pit membrane; see Fig. 1) might also provide for a better seal with the torus of an aspirated pit, because the torus would contact the pit border over a greater area than would be the case with a linear border, where only the torus edge would contact the pit border.

Table 2 Formulas used for resistance calculations

Calculation	Formula
Resistance due to pit borders	$R_{border} = (\Delta p_{border} - \Delta p_{no\ border})/Q$
Resistance due to torus	$R_{torus} = (\Delta p_{torus} - \Delta p_{border})/Q$
Resistance due to margo	$R_{margo} = (\Delta p_{margo} - \Delta p_{torus})/Q$
Resistivity of margo	$r_{margo} = R_{margo} * A_{margo}$; $A_{margo} = \pi(d_{pit}/2)^2 - A_{torus}$
Total pit resistance	$R_{total} = (\Delta p_{margo} - \Delta p_{no\ border})/Q$
Fraction due to aperture	$F_{aperture} = R_{border}/R_{total}$
Fraction due to torus	$F_{torus} = R_{torus}/R_{total}$
Fraction due to margo	$F_{margo} = R_{margo}/R_{total}$

Each expression with Δp refers to the pressure drop occurring in a particular model (indicated by subscript text) and Q is the total volume flow in that model. A_{margo} is the area of the margo, calculated from the pit membrane area (based on pit diameter, d_{pit}) minus the area of the torus as measured from the pit scanning electron microscopy image.

Significant differences were apparent between the flow characteristics of bordered pits of *P. mariana* and *P. glauca*. The pit membranes of *P. mariana* had a 2.3-fold greater intrinsic resistance (resistivity or resistance per unit area) than for *P. glauca*, because the latter species had wider margo pores and greater total pore area. These differences in pit membrane resistivity contributed to a greater margo resistance and total pit resistance among *P. mariana* pits, although the difference in total pit resistance was not statistically significant for the pits sampled. Increasing pit membrane resistivity would contribute to lower xylem conductivity at the stem level; this was in fact observed in a comparative study of these species grown together, where xylem conductivity was expressed on a sapwood and leaf area basis as well as additionally estimated at the plant scale through soil-to-plant hydraulic conductance (Schoonmaker *et al.*, 2010). This partitioning of bordered pit characteristics (which presumably is driving water transport capability) may be of adaptive significance as these species typically occupy very different ecosystems. In Alberta, *P. mariana* commonly occurs in forested peatlands which are nutritionally poor. As the rooting zone depth is correlated with the water table (Lieffers & Rothwell, 1987), periods of drought are exacerbated in peatlands as root systems become completely disconnected from moisture. In addition, peatland soils are cold (e.g. Lieffers & Rothwell, 1987), which further acts to reduce water uptake. In consequence, growth rates are comparatively low and therefore there may be no physiological advantage to high water transport capability. Increased water transport capability is linked with improved growth performance (as recently reiterated in Brodribb, 2009). *P. glauca* tends to occupy sites with better nutrition and moisture regimes (although droughts may still occur), resulting in greater vegetative competition from other species, thus requiring the xylem transport capacity to take advantage of periods of available soil moisture in order to maximize photosynthesis and growth.

As hypothesized, the pits in roots had a significantly lower total resistance than pits in stems, in part because of a greater pore area in addition to the *c.* 1.6-fold greater diameter of the pits found in roots. Domec *et al.* (2006) found higher pit membrane conductivity (lower resistivity) in roots than in stems of *Pseudotsuga*

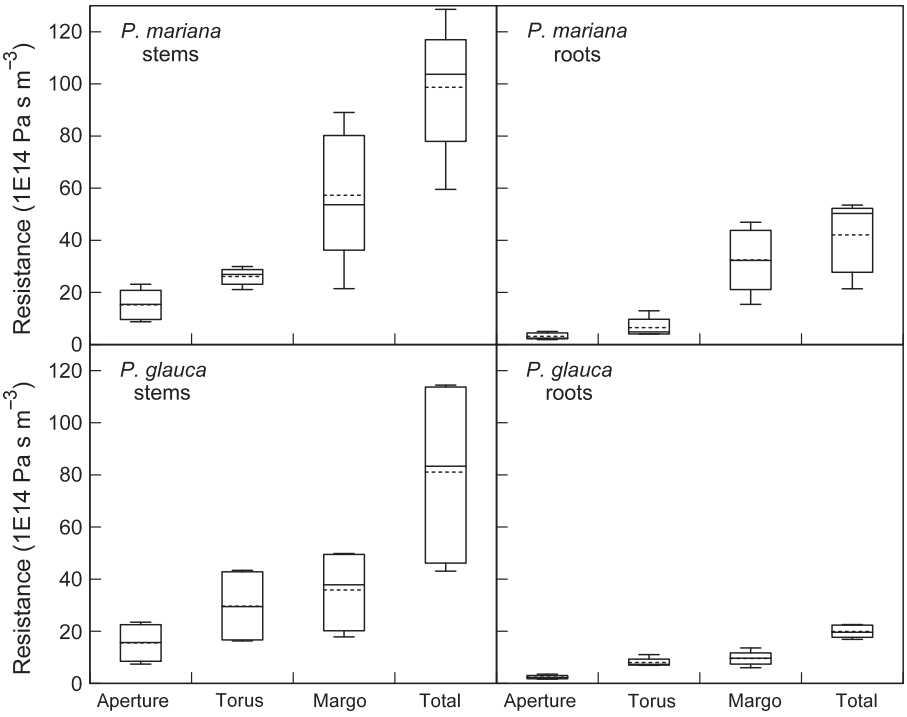

Fig. 6 Hydraulic resistance to flow through the complete pit models for *Picea glauca* and *Picea mariana* as broken down into pit aperture, torus, margo components, and the total pit. For each component of this standard boxplot, the mean is shown as a dashed line, the upper and lower brackets (whiskers) show the maximum and minimum values, and the box shows the 25th, 50th and 75th percentiles from bottom to top.

menziesii, with the margo of pits in roots having a greater average pore diameter. For many conifer species, roots tend to have wider and longer tracheids (Sperry & Ikeda, 1997; Linton *et al.*, 1998; Pittermann *et al.*, 2006; Dunham *et al.*, 2007; Hacke & Jansen, 2009) and these estimates of resistance for pits would then further contribute to lower xylem-specific flow resistance in roots than in stems (Schulte, 2012b).

The pit aperture of bordered pits represents a physical constriction to flow because it is much narrower than the full pit diameter. However, for the pits modeled here, it represented the smallest component of total pit resistance, ranging from 5 to 22%. A similarly low contribution of the pit aperture was indicated by Choat *et al.* (2008). The torus is also a major obstruction to flow. Aside from the obstruction of the pit membrane, the torus is located at what would be the region of greatest flow velocity were it not present. Of course, the role of the torus in its ability to seal the pit when a tracheid becomes air-filled, thus preventing the spread of an embolism (Zimmermann, 1983; Sperry & Tyree, 1990; Hacke *et al.*, 2004; Choat *et al.*, 2008; Delzon *et al.*, 2010), may be of equal importance. For the pits modeled here, the torus was estimated to account for 16–40% of the total pit resistance. For most of the pits modeled, the resistance attributable to the pores of the margo accounted for the greatest fraction of total pit resistance, averaging 44–76% for the two species and stem or root organs. It should be noted that the wide variation observed in measures such as the margo fraction of total pit resistance reflects the observed wide variation in pit margo structure, including pore area, as considered among all the SEM images used for the model development phase of this study. Future studies concerning the role of changes in pit structure with height in tall trees will have to consider the wide variation in pit structure and thus the hydraulic characteristics of pits apparent in the present study. We would suggest that the incorporation of modeling approaches, such as presented in the current study, would help to better understand how the large variation in pit structure (also noted by Valli *et al.*, 2002) might influence flow at the whole organism level.

Pit resistance values from our models can be placed into the context of entire tracheids by utilizing a modeling approach for tracheids that combines pit resistances and lumen resistances into the total resistance to flow (see Hacke *et al.*, 2004; Choat *et al.*, 2008; Schulte, 2012b). Such models assume a 50% overlap between tracheids and consider the tracheid lumen resistance based on tracheid diameter and length along with the pit resistance provided by our models (see Notes S1 for model details). Estimates of average tracheid dimensions and pit numbers for our two species can be obtained from Hacke & Jansen (2009) and Schoonmaker *et al.* (2010). Calculated in this manner, the pit fraction of total tracheid resistance for stems of *P. mariana* and *P. glauca* was 0.431 (range 0.319–0.503) and 0.429 (range 0.301–0.534), respectively. For roots, tracheid dimensions were obtained from Hacke & Jansen (2009), but data on the number of pits per tracheid were not available. An estimate can be made based on the scaling relationships between tracheid length and numbers of pits as observed by Schulte (2012b), although this estimate was developed for Douglas fir and not the two *Picea* species studied here. Incorporating this estimate, the pit fractions of total tracheid resistance for roots of *P. mariana* and *P. glauca* were 0.426 (range 0.283–0.497) and 0.256 (range 0.226–0.281), respectively. Interestingly, the tracheids in roots are wider and longer than those in stems, but the pit fraction of total resistance was approximately the same for stems and roots of

P. mariana. This similarity arose because although the lumen resistance was 6.7-fold higher in stems, the combined resistance of the pits was also 6.7-fold greater (due, in approximately equal measure, to narrower pits with lower pore area and fewer pits per tracheid). The pit fraction for *P. glauca* roots was particularly low, resulting from a roughly twofold lower pit resistance (apparent in Fig. 6) as a result of a nearly twofold greater pore area in the margo of the pits. In general, these estimates of the contribution of the pits to total flow resistance are somewhat lower than previous estimates (Domec *et al.*, 2006; Sperry *et al.*, 2006; Schoonmaker *et al.*, 2010) but somewhat higher than estimated by Lancashire & Ennos (2002) at 29%. Pittermann *et al.* (2006) found that, on average, 64% of the hydraulic resistance of tracheids resided in end-wall pitting and further indicated that this end-wall percentage was independent of tracheid size. Such a scaling relationship as noted earlier for our *P. mariana* stems and roots was similarly explained by Pittermann *et al.* (2006) as resulting from the dependence of the lumen component on tracheid diameter while the pit component depended on tracheid wall area (length and diameter, affecting the number of pits). Domec *et al.* (2010) also found that lumen resistance was related to pit resistance, although the relationship differed between roots and branches of *Pinus taeda*. Therefore, a comparison of pit resistance and lumen resistance components indicates that scaling relationships through tracheid development could act to maintain a nearly constant balance between these two components making up the total resistance to flow through tracheids with torus–margo pits.

Although we cannot use the flow models in this current study to predict how pit membranes will behave at the interface of an air- and water-filled compartment, nonetheless a few tentative statements can be suggested. A large body of literature indicates that tracheids in roots are typically more vulnerable to air-seeding than tracheids in branches (Sperry & Ikeda, 1997; Hacke *et al.*, 2000; Stout & Sala, 2003; Domec *et al.*, 2009). The larger torus–margo pits found in roots would require a structurally stronger margo than found in smaller pits if they were to support the same air-seeding pressure. Greater strength could be achieved by increasing the number of fibrils per area and the diameter of those fibrils, but this would result in greater hydraulic resistance on a margo area basis. In practice, however, thinner margo 'spokes' and larger average pore diameters have been observed in roots than in branches (Domec *et al.*, 2006), suggesting that the reduced structural support provided by the pit margo accounts for their greater vulnerability. This is in agreement with our finding that pits in roots had greater pore area than pits in stems. An examination of shade- and open-grown conifers by Schoonmaker *et al.* (2010) suggested that a relationship between margo pore size and cavitation vulnerability (larger pores associated with increased vulnerability) might indicate a tradeoff between these parameters within a species. On the other hand, Hacke *et al.* (2004) and Pittermann *et al.* (2006) found only a slight relationship between pit conductivity and the air-seed pressure among many northern hemisphere conifers and no correlation was found in southern hemisphere conifers (Pittermann *et al.*, 2006). Pittermann *et al.* (2010) also found that cavitation resistance was not related to the porosity of the margo among conifers in the Cupressaceae. Thus it would seem reasonable to conclude that the size of margo pores among conifers with the torus–margo pit structure is more related to hydraulic resistivity than directly related to xylem vulnerability. Recent work in measuring the force needed to displace the torus and push it against, and ultimately through, the pit aperture indicates that torus flexibility might be an important component in its ability to seal and contain an air-seeding event in conifers with torus-margo pits (Zelinka *et al.*, 2015).

Plavcová *et al.* (2013) recently discussed irregularities in pit structure and suggested that occasionally there may be small 'flaws' or variations in hydrolytic activity during pit development. They suggested that a local excess of hydrolytic activity could result in particularly large pores within the pit membrane. Differences in margo porosity could also influence the ability of pits to repeatedly aspirate and return to the relaxed state. It is conceivable that extremely large pores (such as those in some shade-grown trees; Schoonmaker *et al.*, 2010) with fewer margo fibrils will make membranes more prone to structural damage. This may result in failure of pit membranes to return to their relaxed state when tracheids experience repeated cavitation–refilling cycles. We therefore hypothesize that greater margo pore area, thinner margo 'spokes', and thus lower margo resistance of pits in root tracheids will translate into weaker structural support for an aspirated torus, a factor that may directly result in air-seeding at less negative xylem pressures than in stems. Given the relatively well-established significance of torus-pit aperture scaling for air-seeding (e.g. Domec *et al.*, 2008), we might also expect to find differences in torus-aperture scaling between roots and branches, and this is supported by previous work on *P. glauca* and *P. mariana* (Hacke & Jansen, 2009; Fig. 4 therein). In addition, the distance between pit borders (see Fig. 1) might also contribute to the greater vulnerability of root pits (Hacke & Jansen, 2009; Fig. 5b therein).

We believe that the computational fluid dynamics approach will be a useful one for analyzing flow through pits, as well as perhaps through other structures in the flow pathway. Ongoing further developments will consider a structural mechanics component to the torus–margo, whereby pressure differences across the pit membrane can determine deflection of the pit membrane and ultimately contact between the torus and pit borders. In this manner, future models will be able to couple the fluid and structural aspects of pits. In addition, models can consider a two-phase flow regime for including the presence of air on one side of the pit membrane, as would occur if one tracheid had become embolized. Such models will help in our understanding of how the specific structural details of an individual pit contribute to both fluid flow and protection against the spread of embolism.

Acknowledgements

P.J.S. is grateful to the NSF (DUE-0926678) for support that contributed to this research. We also thank three anonymous

reviewers for their insightful comments, which helped to improve the manuscript.

References

Bauch J, Liese W, Schultze R. 1972. Morphological variability of bordered pit membranes in gymnosperms. *Wood Science and Technology* **6**: 165–184.

Bouche PS, Larter M, Domec J-C, Burlett R, Gasson P, Jansen S, Delzon S. 2014. A broad survey of hydraulic and mechanical safety in the xylem of conifers. *Journal of Experimental Botany* **65**: 4419–4431.

Brodribb TJ. 2009. Xylem hydraulic physiology: the functional backbone of terrestrial plant productivity. *Plant Science* **177**: 245–251.

Chapman DC, Rand RH, Cooke JR. 1977. A hydrodynamical model of bordered pits in conifer tracheids. *Journal of Theoretical Biology* **67**: 11–24.

Choat B, Cobb AR, Jansen S. 2008. Structure and function of bordered pits: new discoveries and impacts on whole-plant hydraulic function. *New Phytologist* **177**: 608–626.

Delzon S, Douthe C, Sala A, Cochard H. 2010. Mechanism of water-stress induced cavitation in conifers: bordered pit structure and function support the hypothesis of seal capillary-seeding. *Plant, Cell & Environment* **33**: 2101–2111.

Domec J-C, Lachenbruch B, Meinzer FC. 2006. Bordered pit structure and function determine spatial patterns of air-seeding thresholds in xylem of Douglas-fir (*Pseudotsuga menziesii*; Pinaceae) trees. *American Journal of Botany* **93**: 1588–1600.

Domec J-C, Lachenbruch B, Meinzer FC, Woodruff DR, Warren JM, McCulloh KA. 2008. Maximum height in a conifer is associated with conflicting requirements for xylem design. *Proceedings of the National Academy of Sciences, USA* **105**: 12069–12074.

Domec J-C, Schäfer K, Oren R, Kim HS, McCarthy HR. 2010. Variable conductivity and embolism in roots and branches of four contrasting tree species and their impacts on whole-plant hydraulic performance under future atmospheric CO_2 concentration. *Tree Physiology* **30**: 1001–1015.

Domec J-C, Warren J, Lachenbruch B, Meinzer FC. 2009. Safety factors from air seeding and cell wall implosion in young and old conifer trees. *IAWA Journal* **30**: 100–120.

Dunham SM, Lachenbruch B, Ganio LM. 2007. Bayesian architecture of Douglas-fir hydraulic architecture at multiple scales. *Trees* **21**: 65–78.

Dute R, Hagler L, Black A. 2008. Comparative development of intertracheary pit membranes in *Abies firma* and *Metasequoia glyptostroboides*. *IAWA Journal* **29**: 277–289.

Dytham C. 2011. *Choosing and using statistics: a biologist's guide*. Oxford, UK: Wiley-Blackwell.

Hacke UG, Jansen S. 2009. Embolism resistance of three boreal conifer species varies with pit structure. *New Phytologist* **182**: 675–686.

Hacke UG, Sperry JS, Ewers BE, Ellsworth DS, Schäfer KVR, Oren R. 2000. Influence of soil porosity on water use in *Pinus taeda*. *Oecologia* **124**: 495–505.

Hacke UG, Sperry JS, Pittermann J. 2004. Analysis of circular bordered pit function II. Gymnosperm tracheids with torus–margo pit membranes. *American Journal of Botany* **91**: 386–400.

Jansen S, Pletsers A, Sano Y. 2008. The effect of preparation techniques on SEM-imaging of pit membranes. *IAWA Journal* **29**: 161–178.

Jensen KH, Zwieniecki MA. 2013. Physical limits to leaf size in tall trees. *Physical Review Letters* **110**: 018104.

Klinka K, Worrall J, Skoda L, Varga P. 2000. *The distribution and synopsis of ecological and silvical characteristics of tree species of British Columbia's forests*. Port Coquitlam, BC, Canada: Canadian Cartographics Ltd.

Koch GW, Sillett SC, Jennings GM, Davis SD. 2004. The limits to tree height. *Nature* **428**: 851–854.

Lancashire JR, Ennos AR. 2002. Modelling the hydrodynamic resistance of bordered pits. *Journal of Experimental Botany* **53**: 1485–1493.

Lieffers VJ, Rothwell RL. 1987. Rooting of peatland black spruce and tamarack in relation to depth of water table. *Canadian Journal of Botany* **65**: 817–821.

Linton MJ, Sperry JS, Williams DG. 1998. Limits to water transport in *Juniperus osteosperma* and *Pinus edulis*: implications for drought tolerance and regulation of transpiration. *Functional Ecology* **12**: 906–911.

Munson BR, Young DF, Okiishi TH. 1990. *Fundamentals of fluid mechanics*. New York, NY, USA: John Wiley & Sons.

Pittermann J, Choat B, Jansen S, Stuart SA, Lynn L, Dawson TE. 2010. The relationships between xylem safety and hydraulic efficiency in the Cupressaceae: the evolution of pit membrane form and function. *Plant Physiology* **153**: 1919–1931.

Pittermann J, Sperry JS, Hacke UG, Wheeler JK, Sikkema EH. 2005. Torus–margo pits help conifers compete with angiosperms. *Science* **310**: 1924.

Pittermann J, Sperry JS, Wheeler JK, Hacke UG, Sikkema EH. 2006. Inter-tracheid pitting and the hydraulic efficiency of conifer wood: the role of tracheid allometry and cavitation protection. *American Journal of Botany* **93**: 1265–1273.

Plavcová L, Hacke UG, Sperry JS. 2011. Linking irradiance-induced changes in pit membrane ultrastructure with xylem vulnerability to cavitation. *Plant, Cell & Environment* **34**: 501–513.

Plavcová L, Jansen S, Klepsch M, Hacke UG. 2013. Nobody's perfect: can irregularities in pit structure influence vulnerability to cavitation? *Frontiers in Plant Science* **4**: 1–6.

Ryan MG, Yoder BJ. 1997. Hydraulic limits to tree height and tree growth. *BioScience* **47**: 235–242.

Schoonmaker AL, Hacke UG, Landhäusser SM, Lieffers VJ, Tyree MT. 2010. Hydraulic acclimation to shading in boreal conifers of varying shade tolerance. *Plant, Cell & Environment* **33**: 382–393.

Schulte PJ. 2012a. Computational fluid dynamics models of conifer bordered pits show how pit structure affects flow. *New Phytologist* **193**: 721–729.

Schulte PJ. 2012b. Vertical and radial profiles in tracheid characteristics along the trunk of Douglas-fir trees with implications for water transport. *Trees* **26**: 421–433.

Sperry JS, Hacke UG. 2004. Analysis of circular bordered pit function. I. Angiosperm vessels with homogenous pit membranes. *American Journal of Botany* **91**: 369–385.

Sperry JS, Hacke UG, Pittermann J. 2006. Size and function in conifer tracheids and angiosperm vessels. *American Journal of Botany* **93**: 1490–1500.

Sperry JS, Ikeda T. 1997. Xylem cavitation in roots and stems of Douglas-fir and white fir. *Tree Physiology* **17**: 275–280.

Sperry JS, Tyree MT. 1990. Water-stress-induced xylem embolism in three species of conifers. *Plant, Cell & Environment* **13**: 427–436.

Stout DL, Sala A. 2003. Xylem vulnerability to cavitation in *Pseudotsuga menziesii* and *Pinus ponderosa* from contrasting habitats. *Tree Physiology* **23**: 43–50.

Valli A, Koponen A, Vesala T, Timonen J. 2002. Simulations of water flow through bordered pits of conifer xylem. *Journal of Statistical Physics* **107**: 121–142.

Woodruff DR, Bond BJ, Meinzer FC. 2004. Does turgor limit growth in tall trees? *Plant, Cell & Environment* **27**: 229–236.

Zelinka SL, Bourne KJ, Hermanson JC, Glass SV, Costa A, Wiedenhoeft AC. 2015. Force displacement measurements of earlywood bordered pits using a mesomechanical tester. *Plant, Cell & Environment*. doi: 10.1111/pce.12532.

Zimmermann MH. 1983. *Xylem structure and the ascent of sap*. New York, NY, USA: Springer.

Supporting Information

Additional supporting information may be found in the online version of this article.

Fig. S1 The full set of pit chamber models based on transmission electron microscopy (TEM) images of pits.

Fig. S2 Volume flow through individual pores of the margo for a pit having a high torus component of resistance.

Fig. S3 Volume flow through individual pores of the torus for a pit having a low torus component of resistance.

Notes S1 Details of the model for relating pit resistance to total tracheid resistance.

Please note: Wiley Blackwell are not responsible for the content or functionality of any supporting information supplied by the authors. Any queries (other than missing material) should be directed to the *New Phytologist* Central Office.